ELSEVIER

International Journal of Mass Spectrometry 225 (2003) 101–114

International Journal of Mass Spectrometry

www.elsevier.com/locate/ijms

Time-of-flight (TOF) mass spectrometer without pulses of any kind, with continuous ion introduction

Gyorgy Hars*, Istvan Maros

Department of Atomic Physics, Budapest University of Technology and Economics, Budafoki ut 8, Budapest H-1111, Hungary

Received 20 June 2002; accepted 21 October 2002

Abstract

A new concept for time-of-flight (TOF) mass spectrometry is presented. Currently, TOF instruments use pulsed ion introduction with a 10 ns or so pulse width, followed by a waiting period roughly 100 μs. Accordingly, the sample is under excitation in 10^{-4} part of the total measuring time, which limits the sensitivity of the method. Secondly, the ion bunch generated is strongly confined, which gives rise to space charge problems deteriorating the signal intensity and the mass resolution.

The concept presented here uses a continuously operating ion source and a special dual modulation technique [Patent pending]. The expected advantages are higher sensitivity and minor space charge limitations. The space charge limitations are obviously easier if the charges are distributed uniformly in an ion beam rather than being confined in a bunch. Moreover, the necessary detection bandwidth is as low as some hundred Hz, which enables to operate the electrometer electronics with amplification as high as 10^{10} V/A. Because of the high signal level, it was possible to omit any electrostatic mirror configuration for bunching the ions. Rather a cylindrical energy filter was installed to remove the ions with undesired energies. The drift tube is roughly 2 m long. The measurement is controlled by a PC via a home made board. The data are collected and the fast Fourier transformation is performed by the software.

The objective of the experimental setup is to demonstrate the operation of this novel measuring principle. The analytical capabilities in present stage are admittedly poor, however its potential improvement is far less limited by physics than in the case of the pulsed TOF techniques.

Keywords: Time-of-flight; Continuos ion introduction; Fourier transformation

1. Introduction

Number of publications deal with the methodical development of time-of-flight (TOF) mass spectrometry [1–16]. A concise overview on the history and the development of this technique was presented by Mamyrin [17].

The operating principle of TOF mass spectrometer is fairly simple. Ions are accelerated by a definite potential and left to run freely in a force-free drift region. Having the same kinetic energy, the smaller the mass. the faster the ion. Ultimately, the first ion to hit the detector will be the lightest, and the order of the arrival will be the monotonic function of the mass number. To make practical use of this principle a definite starting pulse is needed to initiate the flight of the ions.

The width of the starting pulse is in the range of 10 ns, in order to have sufficient mass resolution.

* Corresponding author. Tel.: +36-1-463-4205; fax: +36-1-463-4194.
E-mail address: hars@eik.bme.hu (G. Hars).

1387-3806/02/$ – see front matter © 2002 Elsevier Science B.V. All rights reserved.
PII S1387-3806(02)01060-6

After the starting pulse is fired, a relative long waiting period follows in the range of 100 μs, during which all expected ions reach the detector. Accordingly the duty cycle of the excitation (percentage of the time when the excitation is active) is very low, roughly 10^{-4} part. Because of this, the signal-to-noise ratio is limited, which ultimately limits the sensitivity of the of the measurement.

Due to pulsed excitation the ion packet is strongly confined right after the starting pulse. Though the ions of different mass depart from each other as they travel in the drift region, the ions of the same mass per charge ratio remain together however. The space charge, generated by the ion packet has the unfavorable repelling effect, which might expand the bunch if the drift time is too long. In order to avoid the deterioration of signal level and the mass resolution, a relatively high accelerating voltage is used (4–40 kV). This way the loss of signal can be reduced but the resolution will be limited by the short flight times.

It is clear that using a continuos ion source as opposed to the pulsed one would be advantageous. This kind of ambition motivated Oksman [18] to use continuously operating ion source. He used a specially formulated cylindrical electrostatic field as detector. The signal was low however, since secondary electron multiplier (SEM) could not be used.

2. Theoretical

2.1. Basic formulae

The basic equation for the kinetic energy of an ion is as follows:

$$\tfrac{1}{2}mv^2 = qU \tag{1}$$

where m and q are the mass and charge of the ion, U is the accelerating voltage and v is the velocity of the ion.

The velocity can be readily expressed:

$$v = \sqrt{\frac{2qU}{m}} \tag{2}$$

The time-of-flight τ in a drift region with length L:

$$\tau = \frac{L}{v} = \sqrt{\frac{m}{2qU}} \tag{3}$$

Introducing the atomic mass unit (amu) value M where $m_0 = 1.67 \times 10^{-27}$ kg

$$M = \frac{m}{m_0} \tag{4}$$

(3) is transformed:

$$\tau = \frac{L}{v} = L\sqrt{\frac{m_0}{2qU}}\sqrt{M} \tag{5}$$

Let's introduce A for the flight time of proton.

$$A = L\sqrt{\frac{m_0}{2qU}} \tag{6}$$

Accordingly:

$$\tau = A\sqrt{M}. \tag{7}$$

On the other hand, it is important to know the flight time difference between the neighbor mass numbers. Let's differentiate (7).

$$\frac{\mathrm{d}\tau}{\mathrm{d}M} = \frac{A}{2}\frac{1}{\sqrt{M}} \tag{8}$$

Since the atomic mass unit value is integer, $\mathrm{d}M = 1$. So the flight time difference δ between peaks next to each other is as follows:

$$\delta = \frac{A}{2}\frac{1}{\sqrt{M}} \tag{9}$$

2.2. Theory of the new concept

Assume to have a monoenergetic beam of several different mass over charge ratio ionic species. The total ion current is the sum of the partial currents.

$$I_{\mathrm{tot}} = i_1 + i_2 + \cdots + i_n + \cdots \tag{10}$$

The corresponding flight times in the drift region are

$$\tau_1, \tau_2, \ldots \tau_n \ldots, \text{ respectively.} \tag{11}$$

The intensity of the ion beam can easily be modulated by deflecting the ion beam and conducting it through

an aperture. The ion beam is modulated in intensity in two positions. The first modulation takes place right after the beam is formulated at the beginning of the drift tube. The second modulation (or demodulation if one prefers) happens at the end of the drift region close to the SEM detector. Both modulators are driven with the same RF voltage. The frequency of the driving voltage is increased in small identical increments, starting at 1 MHz or so. The upper limit of the frequency range determines the time resolution, since the reciprocal of the highest frequency is the time between two adjacent points in the Fourier spectrum. One measurement in present case consists of 4096 points.

The modulating functions are as follow:

$$A(\omega)\,\mathrm{mod}(\omega t) \quad \text{and} \quad B(\omega)\,\mathrm{Mod}(\omega t) \tag{12}$$

where mod(ωt) and Mod(ωt) are periodic functions in $2\pi/\omega$. $A(\omega)$ and $B(\omega)$ are the corresponding amplitudes as the function of the modulating angular frequency. The modulators are driven with the identical pure cosine function deflection voltage. The two modulating functions in (12) are not necessarily cosine, due to the possible nonlinearity between the deflection voltage and the modulated intensity of the transmitted ion beam. In ideal case however these functions were pure cosine. So, by introducing (12) functions the nonlinearity of the modulation process can be taken into account.

The frequency dependence of the amplitudes $A(\omega)$ and $B(\omega)$ is the conclusion of the frequency dependence of the analog electronics involved, which consists of the high frequency drive amplifier and the ferrite transformer of the modulator (Fig. 1).

All analog electronics has amplitude characteristic. This is the output amplitude of the device, provided a constant amplitude sinusoidal signal was applied to its input, and the frequency of the input signal is swept through the relevant range.

In present case a frequency-independent amplitude characteristic would be ideal. In other words the graph of the amplitude characteristic supposed to be a horizontal line. Since the experimental setup in present stage is not at the level of an analytical equipment, the amplitude characteristic is not ideal, so $A(\omega)$ and $B(\omega)$ amplitudes depend on the frequency.

The operation called modulation is in fact analog multiplication in terms of mathematics. Right after the first modulation the ion current as a function of time $I_1(t)$ is as follows:

$$I_1(t) = (i_1 + i_2 + \cdots + i_n + \cdots)A(\omega)\,\mathrm{mod}(\omega t) \tag{13}$$

At the end of the drift region right before the second modulation the ion current $I_2(t)$ is:

$$I_2(t) = A(\omega)\{i_1\,\mathrm{mod}[\omega(t-\tau_1)] + \cdots + i_n\,\mathrm{mod}[\omega(t-\tau_n)] + \cdots\} \tag{14}$$

After the second modulation the ion current $I_3(t)$ is as follows:

$$I_3(t) = A(\omega)B(\omega)\left\{\sum_{k=1}^{\infty} i_k\,\mathrm{mod}[\omega(t-\tau_k)]\,\mathrm{Mod}(\omega t)\right\} \tag{15}$$

The modulating functions are represented by the cosine Fourier series:

$$\mathrm{mod}[\omega(t-\tau_k)] = a_0 + a_1\cos[\omega(t-\tau_k)] + a_2\cos[2\omega(t-\tau_k)] + a_3\cos[3\omega(t-\tau_k)] + \cdots \tag{16}$$

$$\mathrm{Mod}(\omega t) = b_0 + b_1\cos\omega t + b_2\cos 2\omega t + \cdots \tag{17}$$

Consider the k-th ionic species for a moment. Here two series (16) and (17) is to be multiplied together. All those products will be time-dependent where the factors belong to different frequencies, thus these products will disappear after low pass filtering. Factors with same frequency however, will provide dc product after low pass filtering. The dc result is the half of the product of the corresponding amplitudes. Here the following elementary rule was used:

$$\cos\alpha\cos\beta = \tfrac{1}{2}[\cos(\alpha+\beta) + \cos(\alpha-\beta)] \tag{18}$$

Following the second modulation, the dc result or in other words the time average of the total ion beam,

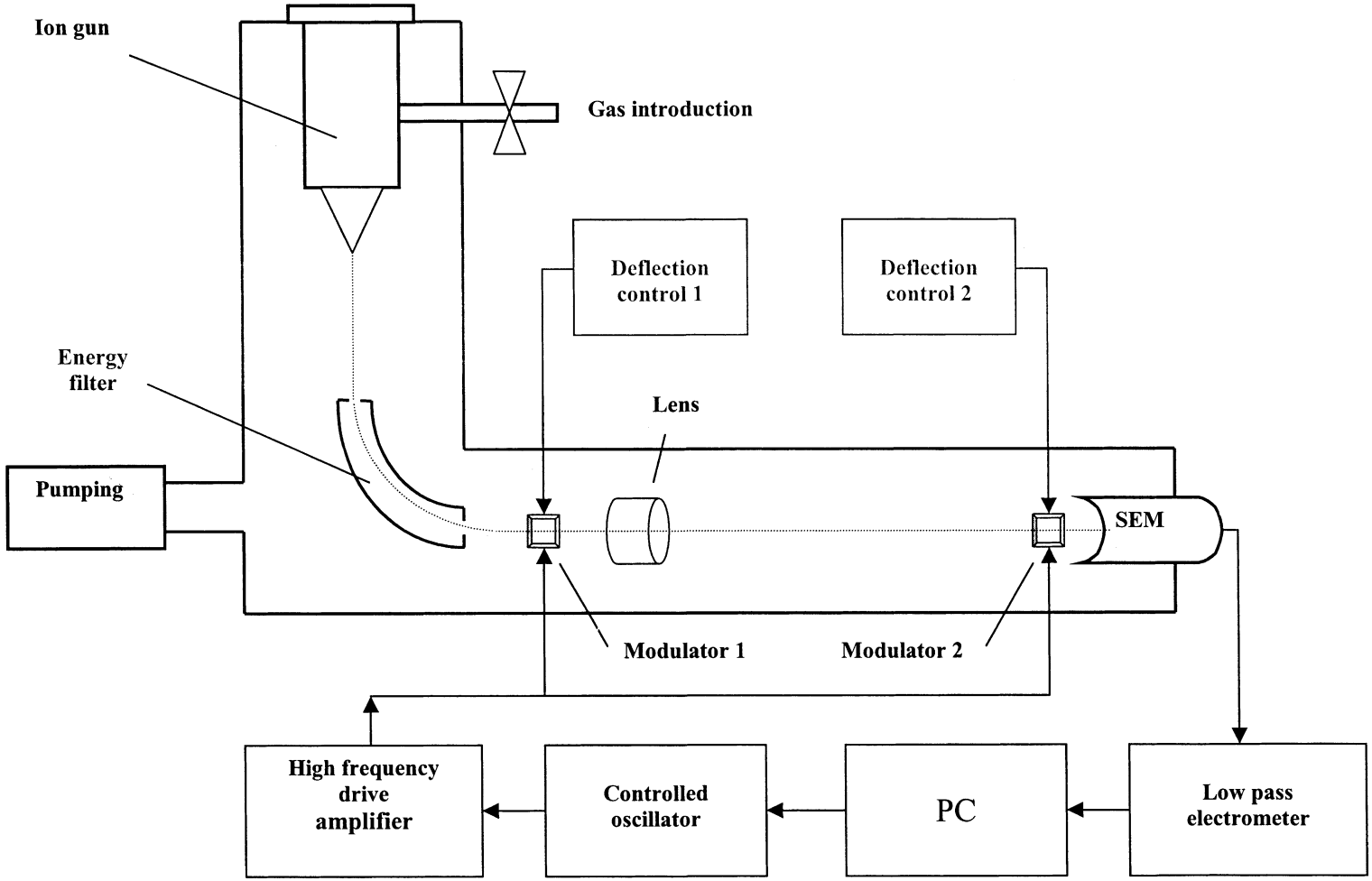

Fig. 1. TOF MS with continuous ion introduction. Schematic arrangement of the experimental setup.

considering all ionic species is as follows:

$$K(\omega) = \frac{A(\omega)B(\omega)}{2}\sum_{k=1}^{\infty} i_k[a_0b_0 + a_1b_1\cos(\omega\tau_k) + a_2b_2\cos(2\omega\tau_k) + \cdots + a_nb_n\cos(n\omega\tau_k) + \cdots] \quad (19)$$

One of the modulators at least must be operated in linear range. Let us choose the second modulator. $\mathrm{Mod}(\omega t) = b_0 + \cos\omega t$ which means $b_2 = b_3 = \cdots b_n = 0$.

$$K(\omega) = \frac{A(\omega)B(\omega)}{2}\sum_{k=1}^{\infty} i_k[a_0b_0 + a_1b_1\cos(\omega\tau_k)] \quad (20)$$

Here $R(\omega)$ function is introduced, which characterizes the amplitude characteristic of the linearized measuring system. $R(\omega) = A(\omega)B(\omega)/2$ by means of this

$$K(\omega) = R(\omega)\sum_{k=1}^{\infty} i_k[a_0b_0 + a_1b_1\cos(\omega\tau_k)] \quad (21)$$

$$K(\omega) = R(\omega)\{a_0b_0I_{\mathrm{tot}} + a_1b_1[i_1\cos(\omega\tau_1) + i_2\cos(\omega\tau_2) + \cdots + i_n\cos(\omega\tau_n)]\} \quad (22)$$

Disregard the frequency-independent terms:

$$K(\omega) = R(\omega)a_1b_1[i_1\cos(\omega\tau_1) + i_2\cos(\omega\tau_2) + \cdots + i_n\cos(\omega\tau_n)] \quad (23)$$

The $R(\omega)$ frequency dependence can be compensated by carrying out a measurement with only one ionic species in the drift region. The corresponding drift time is τ_1.

$$K(\omega) = R(\omega)a_1b_1i_1\cos(\omega\tau_1) \quad (24)$$

The result of (24) is different of pure cosine function due to $R(\omega)$ alone. Accordingly, a compensating function can be made which is proportional to the reciprocal of $R(\omega)$. The compensation is carried out by the computer after data collection. For later processing the compensated function $K^*(\omega)$ is used:

$$K^*(\omega) = i_1\cos(\omega\tau_1) + i_2\cos(\omega\tau_2) + \cdots + i_n\cos(\omega\tau_n) \quad (25)$$

$$K^*(f) = i_1\cos(2\pi f\tau_1) + i_2\cos(2\pi f\tau_2) + \cdots + i_n\cos(2\pi f\tau_n) \quad (26)$$

Performing Fourier transformation on (26) by f frequency the partial ion currents appear at the corresponding flight times, which is the TOF spectrum of the ion beam. The Fourier transformation is carried out by the computer with an FFT algorithm.

2.3. Theory of the equipment engineering

The reciprocal value of the highest frequency is the "time quantum τ_0", which determines the time resolution.

$$\frac{1}{f_{\max}} = \tau_0 \quad (27)$$

dividing the time of flight in (7) with the time quantum the corresponding channel number k results.

$$\frac{\tau}{\tau_0} = k \quad (28)$$

$$k = Af_{\max}\sqrt{M} \quad (29)$$

In order to avoid aliasing, only the first half of the FFT result can be used. That means for Fourier transformation with $n = 4096$, where n is the number of data input to the FFT algorithm, the useable output data are the first 2048 points.

$$\frac{n}{2} = Af_{\max}\sqrt{M_{\mathrm{range}}} \quad (30)$$

$$\left(\frac{n}{2Af_{\max}}\right)^2 = M_{\mathrm{range}} \quad (31)$$

Here M_{range} denotes the mass range of the method.

A mass peak can be considered resolved if two time quanta elapsed between neighbor mass numbers at least. This definition makes possible to find the peak and the valley. According to formula (9) $2\tau_0 = \delta$.

$$\frac{2}{f_{\max}} = \frac{A}{2}\frac{1}{\sqrt{M_{\mathrm{res}}}} \quad (32)$$

$$\left(\frac{Af_{\max}}{4}\right)^2 = M_{\mathrm{res}} \quad (33)$$

Here M_{res} denotes the highest mass number resolved.

In ideal case the total mass range is resolved. $M_{\text{range}} = M_{\text{res}}$. This leads to the condition to determine the highest frequency necessary.

$$\left(\frac{n}{2Af_{\max}}\right)^2 = \left(\frac{Af_{\max}}{4}\right)^2 \tag{34}$$

$$f_{\max} = \frac{\sqrt{2n}}{A} \tag{35}$$

Using this frequency (36) results:

$$M_{\text{range}} = M_{\text{res}} = \frac{n}{8} \tag{36}$$

Longitudinal dimension of the deflection plates is crucial. This is denoted L^*. The ratio between the total flight length L and this dimension is p (in the order of thousand).

$$\frac{L}{L^*} = p \tag{37}$$

The deflection of the ion beam starts to diminish abruptly once the half period of the modulating signal becomes equal to the duration that an ion spends between the deflection plates.

$$\frac{A}{p}\sqrt{M_{\text{defl}}} = \frac{1}{2f_{\max}} \tag{38}$$

This effect makes indispensable to use the possible shortest dimension of the deflector parallel with the ion beam. Here the highest mass number possible to be deflected is denoted with M_{defl}

$$\left(\frac{p}{2Af_{\max}}\right)^2 = M_{\text{defl}} \tag{39}$$

In order to satisfy the obvious requirement that $M_{\text{range}} = M_{\text{defl}}$

$$\left(\frac{n}{2Af_{\max}}\right)^2 = \left(\frac{p}{2Af_{\max}}\right)^2 \tag{40}$$

From (40) $n = p$ results. This means, that the number of elementary measuring cycles in one measurement should be the same as the ratio between the length of the drift region and the longitudinal dimension of the deflection plates.

The needed bandwidth of the low pass electrometer is dependent on the time period Δ between the frequency increments. The average angular acceleration β is the ratio of the change in angular frequency and the elapsed time.

$$\beta = 2\pi\frac{f_{\max}}{n\Delta} \tag{41}$$

Thus the angular frequency can be expressed as follows:

$$\omega = \beta t \tag{42}$$

Consider (25) and substitute (42). This way $K^*(\omega)$ is converted to $K^*(t)$ time function.

$$K^*(t) = i_1\cos(\beta\tau_1 t) + i_2\cos(\beta\tau_2 t) + \cdots + i_n\cos(\beta\tau_n t) \tag{43}$$

Here the corresponding $\beta\tau$ products are the angular frequencies denoted with Ω.

$$K^*(t) = i_1\cos(\Omega_1 t) + i_2\cos(\Omega_2 t) + \cdots + i_n\cos(\Omega_n t) \tag{44}$$

The angular frequency corresponding to a certain M mass number according to (7) is as follows:

$$\Omega = \beta A\sqrt{M} \tag{45}$$

Substituting (41):

$$\Omega = 2\pi\frac{Af_{\max}}{n\Delta}\sqrt{M} \tag{46}$$

Switching to frequency ($F = \Omega/2\pi$):

$$F = \frac{Af_{\max}}{n\Delta}\sqrt{M} \tag{47}$$

For $M = 1$ is the lowest frequency $F_{\min}$

$$F_{\min} = \frac{Af_{\max}}{n\Delta} \tag{48}$$

For $M = M_{\text{range}}$ the highest frequency $F_{\max}$:

$$F_{\max} = \frac{Af_{\max}}{n\Delta}\sqrt{M_{\text{range}}} \tag{49}$$

The above two formulae determine the necessary bandwidth of the low pass electrometer. It is clear

that full dc transmission is not required. This justifies the step between (22) and (23) when the frequency-independent terms were disregarded.

Interesting interpretation of the method becomes apparent by considering formulae (43) and (44) more in detail. If the frequency sweep were not happening in stepwise manner but would be continuos, the generated angular frequencies were the results of the product of cosine and an earlier cosine, which has lower frequency due to the frequency sweep. The resulting signal has the frequency which is the difference of the frequencies of those signals multiplied together.

The shortest possible duration between frequency increments is determined by the need that during this time the ions with the highest mass must reach the detector.

In terms of mathematics:

$$\Delta = A\sqrt{M_{\text{range}}} \tag{50}$$

Substituting (50) to (48) and (49) the highest possible values of $F_{\min}$ and $F_{\max}$ results:

$$F_{\min} = \frac{f_{\max}}{n}\frac{1}{\sqrt{M_{\text{range}}}} \tag{51}$$

$$F_{\max} = \frac{f_{\max}}{n} \tag{52}$$

The shortest possible duration for spectrum recording $T_{\min}$ is as follows:

$$T_{\min} = nA\sqrt{M_{\text{range}}} \tag{53}$$

3. Experimental

The experimental setup was built to prove the concept (Fig. 1). The setup consists of the following major parts: vacuum chamber, ion gun, energy filter, Einzel lens, SEM detector, modulator 1, modulator 2, deflection control 1, deflection control 2, high frequency drive amplifier, controlled oscillator, low pass electrometer, PC. During measurements the vacuum was in the order of 10^{-6} mbar.

The ion gun provided 100 nA primary beam current at 1 kV beam voltage. The deflection and focus functions of the ion gun were used to supply maximum current to the outer cylinder of the energy selector (see Fig. 1). This current was roughly 80 nA. This way the system could be adjusted in separate steps.

The inner cylinder of the energy selector was internally grounded. Once the first part was adjusted, 560 V was hooked up to the outer cylinder. The signal at the output of the low pass electrometer was maximized by tuning the modulators with the corresponding deflection control and by adjusting the voltage of the energy selector and the Einzel lens.

Modulator in its original concept is no more than a pair of deflection plates followed by an aperture. The intensity of the ion beam can easily be modulated by deflecting the ion beam and conducting it through an aperture. There are two fundamental limitations, however.

The modulation is not a linear process. It means that by driving the modulator with cosine function, the modulated beam intensity will not be cosine. This effect can be diminished by using little modulation amplitudes and using slit-like aperture. Other major limiting factor is the time during which the ion travels in the deflector. It is obvious, that when this duration becomes equal to the period of the modulating voltage, deflection will not occur. This means that the modulators must have a very small extension parallel with the ion beam in order to reach sufficiently high modulation frequency. Practically the deflectors are a pair of thin metal sheets in the same plane making a slit of 1 mm or so. They are covered on both sides with similar size grounded metal sheet forming the same slit in order to shield the electric field from the approaching and departing ion. Following the deflection there is the aperture, which is a grounded metal slit parallel with the deflector slit and about twice wider and it is about 20–25 mm distance from the deflector.

The actual measurement takes place by increasing the modulation frequency from 1 up to 8 MHz in 4096 uniform steps. The maximum frequency is limited to 8 MHz by the deflecting ferrite transformers. In addition the deflection amplitude was constantly changing as the frequency increased. Strict regulation will be needed later on to keep deflection voltage constant.

The output of the low pass electrometer is recorded at all frequencies. One such cycle lasts 3 ms, so the measurement takes about 13 s. The collected data are compensated for the frequency dependence of the deflection electronics by multiplying it with the compensating function. This is followed by the fast Fourier transformation (FFT) algorithm. The software displays only the first 2048 points of the FFT result.

The major equipment parameters for the case of the existing experimental setup are calculated below:

The flight time of proton A is as follows (6):

$$A = L\sqrt{\frac{m_0}{2qU}} = 4.82\,\mu\text{s} \tag{54}$$

where $m_0 = 1.67 \times 10^{-27}$ kg, $q = 1.6 \times 10^{-19}$ A, $U = 10^3$ V, $L = 2.1$ m.

The FFT channel number as a function of the amu value (29).

$$k = Af_{\max}\sqrt{M} = 38.55\sqrt{M} \tag{55}$$

where $A = 4.82\,\mu$s, $f_{\max} = 8$ MHz.

The mass range in (31):

$$\left(\frac{n}{2Af_{\max}}\right)^2 = M_{\text{range}} = 2822\,\text{amu} \tag{56}$$

where $n = 4096$.

The highest mass number resolved: M_{res} in (33).

$$\left(\frac{Af_{\max}}{4}\right)^2 = M_{\text{res}} = 92\,\text{amu} \tag{57}$$

The needed frequency to match mass range to the highest resolved mass value (35).

$$f_{\max} = \frac{\sqrt{2n}}{A} = 18.8\,\text{MHz} \tag{58}$$

If the frequency had been 18.8 MHz the resolved mass range would be 512 amu in (36). It is clear that the mismatch between the values in (56) and (57) is due to the fact that the maximum frequency is 8 MHz only.

From (40), $n = p$ results. This means that the ratio between the length of the drift region (which is 2.1 m here) and the longitudinal dimension of the deflection plates should be 4096. This limits the longitudinal length of the deflectors to roughly 0.5 mm.

The minimum signal frequency according to (48) which determines the lower frequency limit of the low pass electrometer:

$$F_{\min} = \frac{Af_{\max}}{n\Delta} = 3.1\,\text{Hz} \tag{59}$$

where $\Delta = 3$ ms, the time between frequency increments. The 3 ms value is far longer than the theoretical minimum in formula (50).

The signal frequency at any mass number M according to (47) is as follows:

$$F = 3.1\,\text{Hz}^*\sqrt{M} \tag{60}$$

The maximum signal frequency at the top of the mass range according to (56) which determines the higher frequency limit of the low pass electrometer is as follows:

$$F_{\max} = 3.1\,\text{Hz}^*\sqrt{2822} = 165\,\text{Hz} \tag{61}$$

4. Results and discussion

The operation of the setup was demonstrated on air intentionally introduced. The background pressure was 10^{-6} mbar, the introduced air represented 7×10^{-6} mbar. Two measurements of the same gas composition are presented to show the phases of the data acquisition and to have an impression about the reproducibility.

The expected minor components are the usual water vapor at 18 amu and some carbon dioxide at 44 amu.

Figs. 2 and 3 show the collected data for the two measurements. This absolutely does not resemble to any spectrum, rather a combination of sine functions. At Air3007 measurement a saturation of the PC board happened which cut some of the signal.

Fig. 4 displays the computer simulation of that fictive measurement if only nitrogen at 28 amu and oxygen at 32 amu appeared in the spectrum in a ratio equal to the natural air. This shows a substantial similarity to the real records of Figs. 2 and 3.

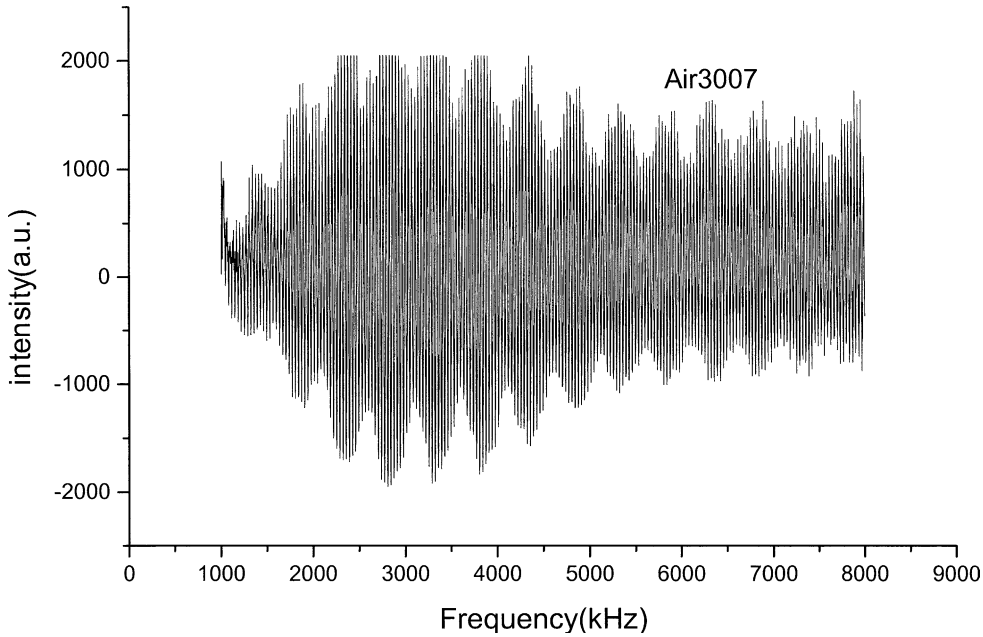

Fig. 2. The output of the low pass electrometer as a function of the modulating frequency, recorded on air. Test number 3007.

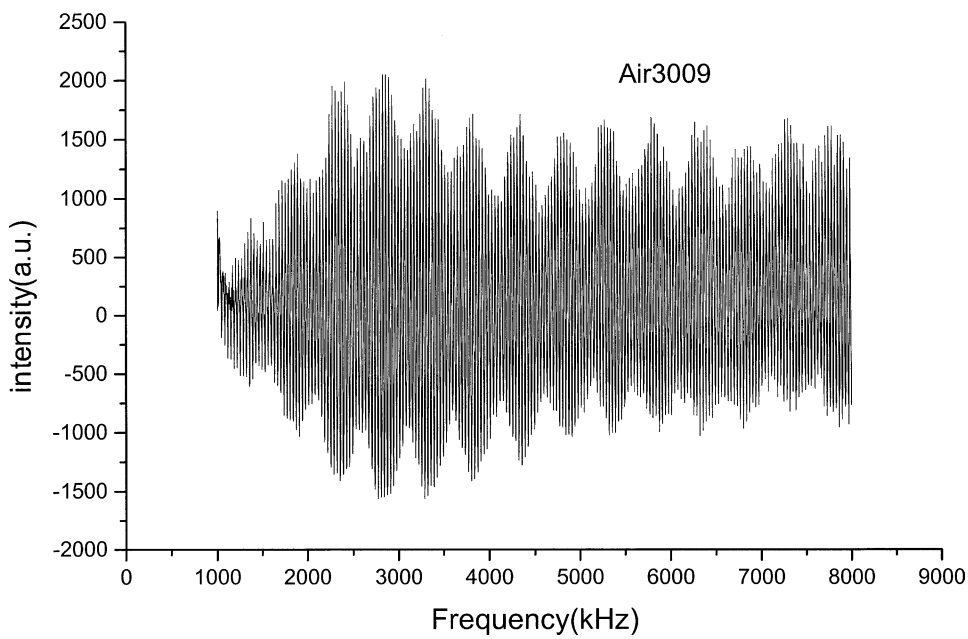

Fig. 3. The output of the low pass electrometer as a function of the modulating frequency, recorded on air. Test number 3009.

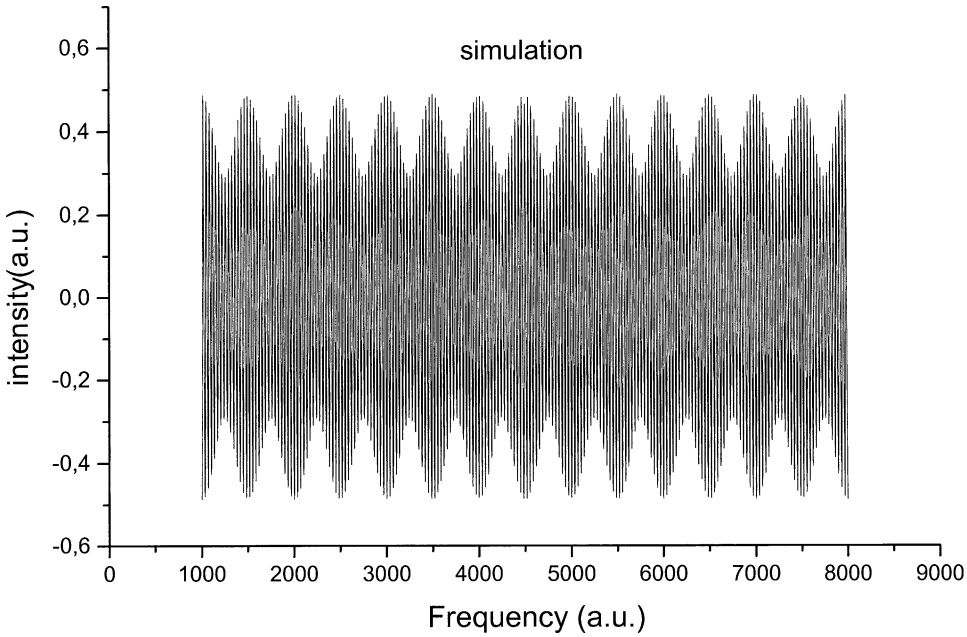

Fig. 4. Computer simulation of a virtual measurement if only N_2 at 28 amu and O_2 at 32 amu were present, in the ratio of the natural air.

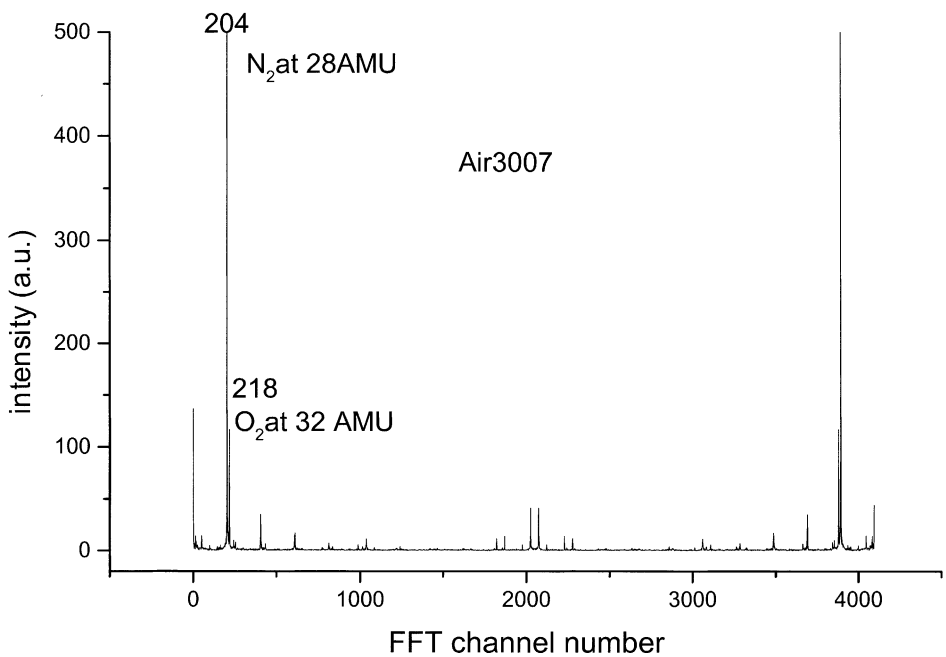

Fig. 5. Direct result of the FFT algorithm on test 3007.

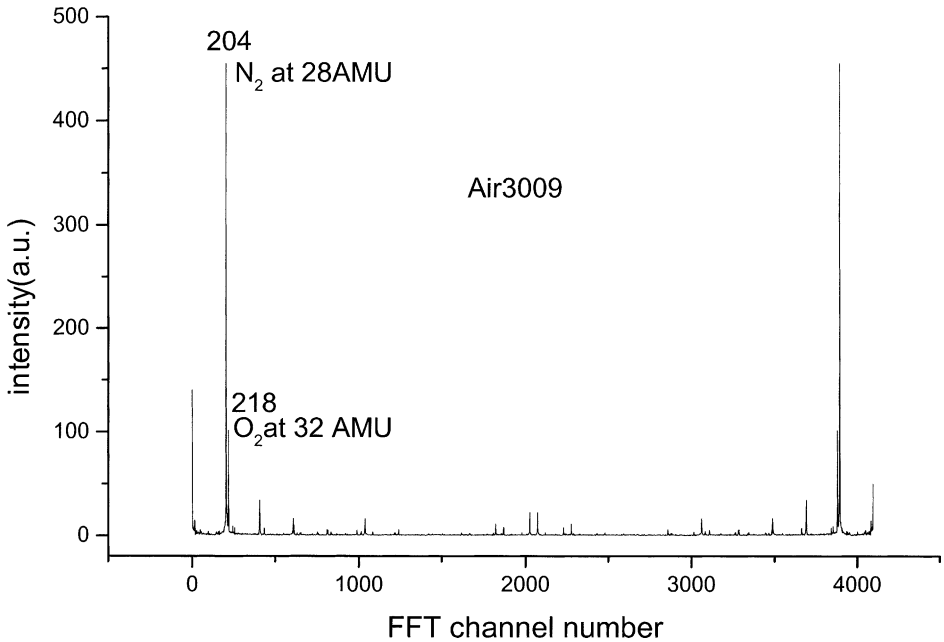

Fig. 6. Direct result of the FFT algorithm on test 3009.

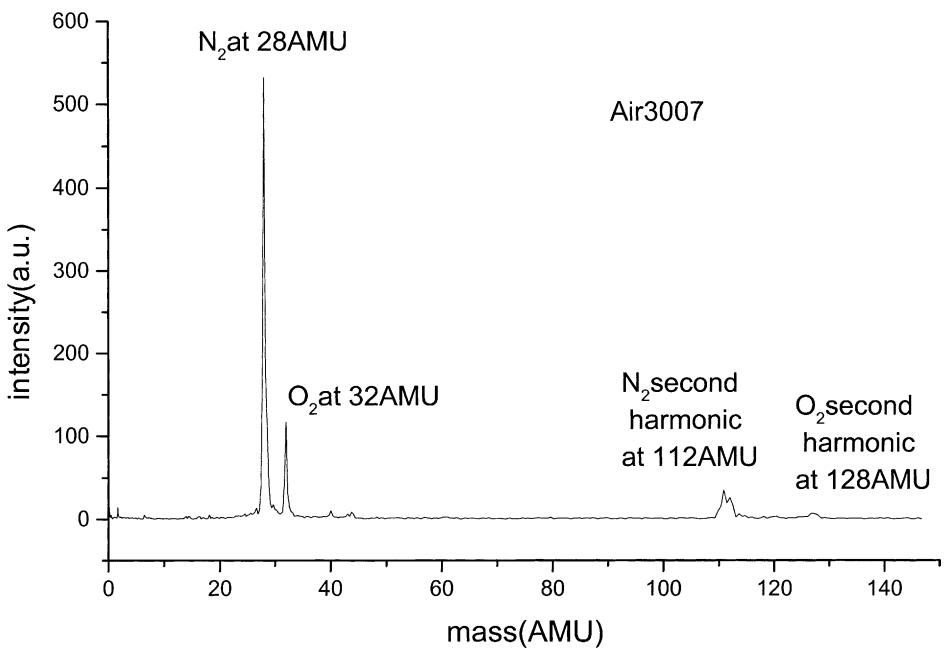

Fig. 7. Linear mass spectrum of air up to 150 amu at test 3007.

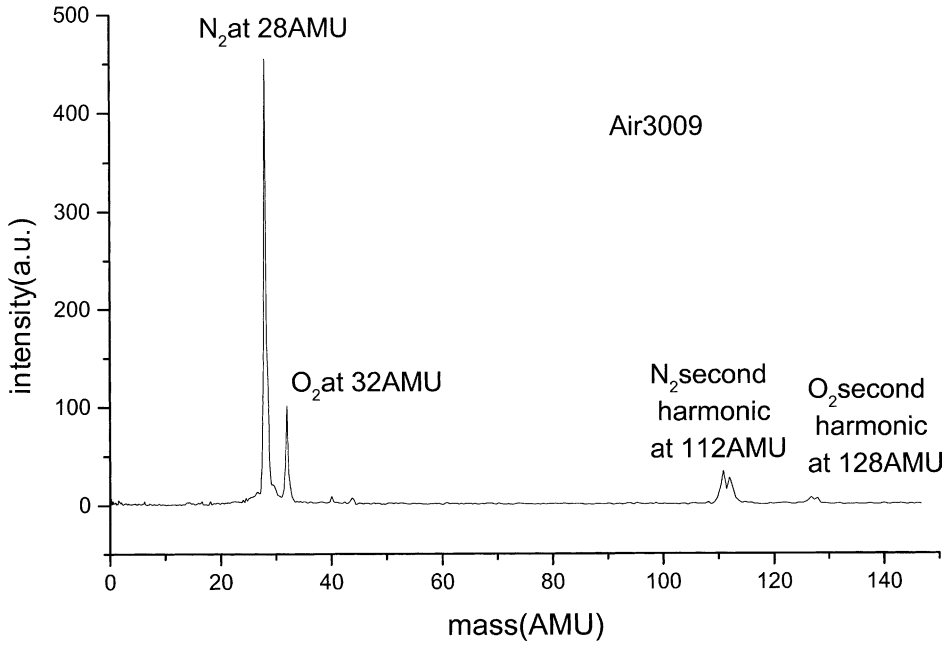

Fig. 8. Linear mass spectrum of air up to 150 amu at test 3009.

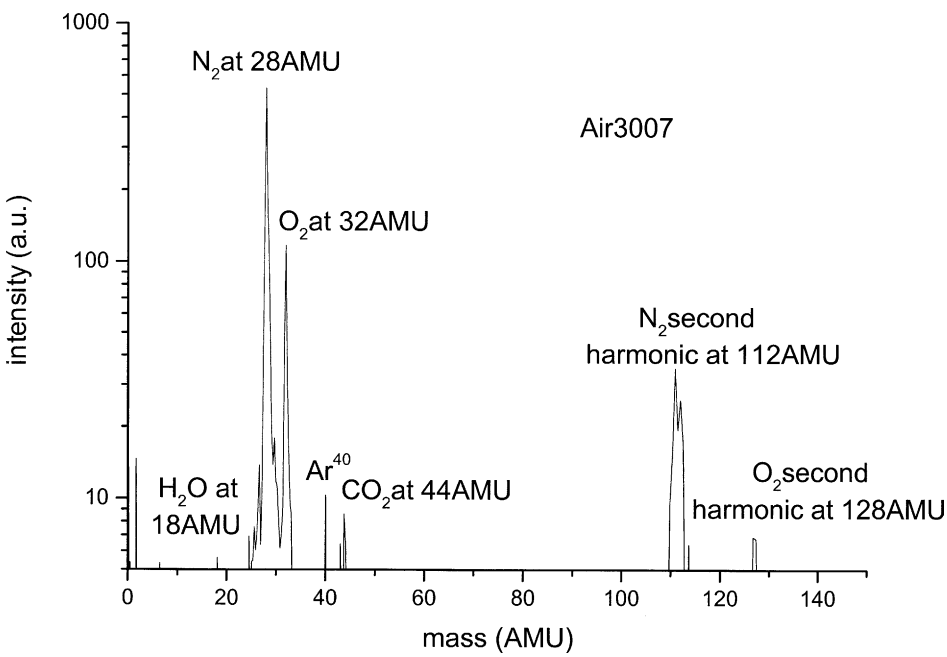

Fig. 9. Logarithmic mass spectrum of air up to 150 amu at test 3007.

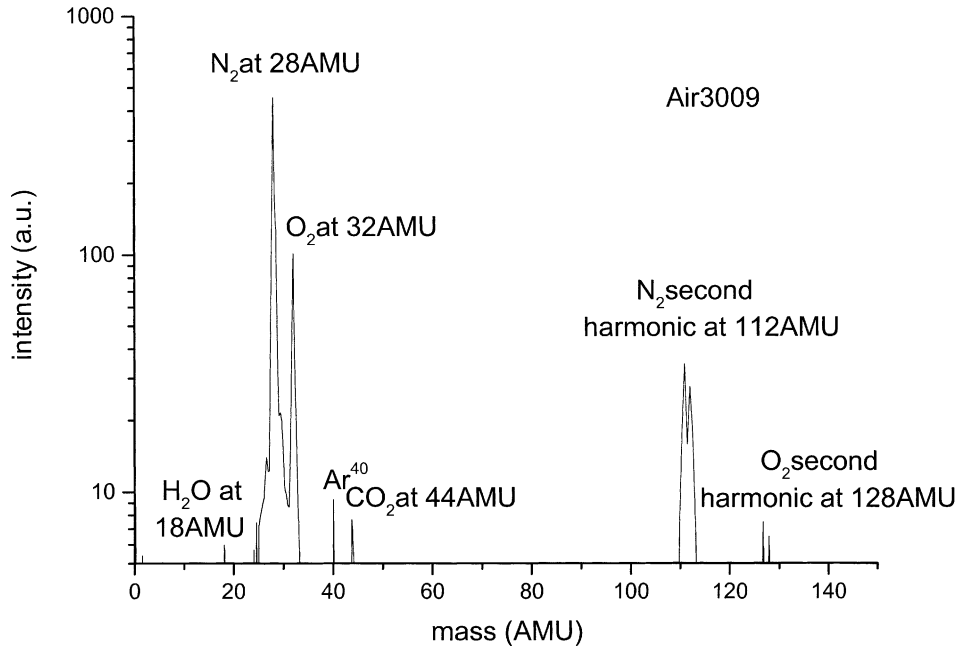

Fig. 10. Logarithmic mass spectrum of air up to 150 amu at test 3009.

The FFT transformation of Figs. 2 and 3 resulted in Figs. 5 and 6. These contain 4096 points and they are symmetrical due to the properties of the Fourier transformation.

The software has been further developed. The horizontal axis was converted to amu scale. Figs. 7 and 8 show the spectra up to 150 amu with the intensity on linear scale. The same spectra are displayed with the intensity on logarithmic scale on Figs. 9 and 10. Intensity values under five were ignored. Here the following components can be recognized. The peaks of nitrogen at 28 amu and oxygen at 32 amu clearly show up. Roughly the nitrogen is five times bigger, which is the expected ratio, similar to natural air. Peaks of carbon dioxide at 44 amu and some residue of argon at 40 amu is also visible. Minor peak of water vapor shows up at 18 amu in both cases. Interesting to find the second harmonic of nitrogen and oxygen at 112 and at 128 amu. The second harmonic signal shows up at double FFT channel number, which ultimately corresponds to a four times higher mass value. This is a warning signal that the modulators do not satisfy the condition that one of them supposed to work in linear mode. This must be improved later on.

5. Conclusions

A new concept has been presented for time-of-flight mass spectrometry. The suggested concept uses continuos ion introduction as opposed to the pulsed ion introduction which is generally used. This way the signal-to-noise performance of the method is thought to be improved due to the fact that the analyte is under constant excitation. The space charge limitations are similarly eased since the ions are not confined in a bunch but in a continuos ion beam. Furthermore, because of the combined modulation demodulation technique, the high frequency ion signal needs not to be transmitted through the SEM and the electrometer, since the signal is mixed back to the base band in the vacuum chamber. This way very high amplification can be applied at the electrometer which also improves the sensitivity.

Critical point of the method is the longitudinal dimension of the deflectors, which must be kept small. Other important point is the linearity of the modulation. Due to nonlinear modulation higher harmonic peaks appear in the spectrum.

Acknowledgements

The authors wish to thank to Lajos Bori and Bela Piel for their very important contribution in making the vacuum parts as well as the PC board and the software.

References

[1] E.N. Nikolaev, V.S. Rakov, R.E. Tosh, A.K. Shukla, J.H. Futrell, ICR/Ion Trap Newsletter 44 (Autumn 1996) 14.
[2] J.M. Grundwüzner, M. Bönisch, G.R. Kinsel, J. Grotemeier, E.W. Schlag, Int. J. Mass Spectrom. Ion Process. 131 (1994) 139.
[3] C. Brunne, Int. J. Mass Spectrom. Ion Process. 76 (1987) 125.
[4] B.A. Mamyrin, Int. J. Mass Spectrom. Ion Process. 131 (1994) 1.
[5] T. Bergman, T.P. Martin, H. Schaber, Rev. Sci. Instrum. 60 (1989) 347.
[6] T. Bergman, T.P. Martin, H. Schaber, Rev. Sci. Instrum. 60 (1989) 214.
[7] T. Bergman, H. Goehlich, T.P. Martin, H. Schaber, G. Malegiannakis, Rev. Sci. Instrum. 61 (1990) 2585.
[8] T. Bergman, T.P. Martin, H. Schaber, Rev. Sci. Instrum. 61 (1990) 2592.
[9] V.M. Doroshenko, R.J. Cotter, J. Am. Soc. Mass Spectrom. 10 (1999) 992.
[10] M. Yang, J.P. Reilly, Int. J. Mass Spectrom. Ion Process. 75 (1987) 209.
[11] U. Boesl, R. Wenkauf, E.W. Schlag, Int. J. Mass Spectrom. Ion Process. 112 (1992) 121.
[12] H. Wollnik, M. Przewloka, Int. J. Mass. Spectrom. Ion Process. 96 (1990) 267.
[13] A. Casares, A. Kholomeev, H. Wollnik, Int. J. Mass. Spectrom. 206 (2001) 267.
[14] C.S. Hoaglund, S.J. Valentine, C.R. Sporleder, J.P. Reilly, D.E. Clemmer, Anal. Chem. 70 (1998) 2236.
[15] A.F. Dodonov, V.I. Kozlovski, I.V. Soulimenkov, V.V. Raznikov, A.V. Loboda, T. Horwath, H. Wollnik, Euro. J. Mass Spectrom. 6 (6) (2000) 481.
[16] E.R. Badman, R.G. Cooks, J. Mass Spectrom. 35 (2000) 659.
[17] B.A. Mamyrin, Int. J. Mass Spectrom. 206 (2001) 251.
[18] P. Oksman, Int. J. Mass Spestrom. 141 (1995) 67.